

Two dimensional bright solitons in dipolar Bose-Einstein condensates with tilted dipoles

Meghana Raghunandan,¹ Chinmayee Mishra,¹ Kazimierz Łakomy,² Paolo Pedri,^{3,4} Luis Santos,² and Rejish Nath¹

¹Indian Institute of Science Education and Research, Pune 411 008, India

²Institut für Theoretische Physik, Leibniz Universität Hannover, Appelstrasse 2, DE-30167 Hannover, Germany

³Université Paris 13, Sorbonne Paris Cité, Laboratoire de Physique des Lasers, F-93430 Villetaneuse, France

⁴CNRS, UMR 7538, LPL, F-93430 Villetaneuse, France

(Dated: December 10, 2021)

The effect of dipolar orientation with respect to the soliton plane on the physics of two-dimensional bright solitons in dipolar Bose-Einstein condensates is discussed. Previous studies on such a soliton involved dipoles either perpendicular or parallel to the condensate-plane. The tilting angle constitutes an additional tuning parameter, which help us to control the in-plane anisotropy of the soliton as well as provides access to previously disregarded regimes of interaction parameters for soliton stability. In addition, it can be used to drive the condensate into phonon instability without changing its interaction parameters or trap geometry. The phonon-instability in a homogeneous 2D condensate of tilted dipoles always features a transient stripe pattern, which eventually breaks into a metastable soliton gas. Finally, we demonstrate how a dipolar BEC in a shallow trap can eventually be turned into a self-trapped matter wave by an adiabatic approach, involving the tuning of tilting angle.

I. INTRODUCTION

Last two decades have witnessed intensive investigations, both theoretical and experimental, on multi-dimensional solitons, especially in systems possessing *nonlocal nonlinearity* (NLNL) [1–3] such as Bose-Einstein condensates (BECs) of particles with permanent [4, 5] or induced dipole moments [6] (*dipolar BECs*), photo refractive materials [7], nematic liquid crystals [8, 9] and others [10–12]. Two-dimensional (2D) optical bright solitons [13] and three-dimensional (3D) light bullets [14] have been reported in non-local media. In addition, nonlocal interactions significantly influence inter-soliton collisions [4, 7, 15, 16] and may lead to the formation of soliton complexes [17, 18].

Bright solitons in BECs have been realized experimentally only in quasi-1D alkali-atom gases [19–21], in which short-range contact-like interactions result in a cubic nonlinearity equivalent to self-focusing nonlinearity in a Kerr media. Whereas in these media higher-dimensional solitons are unstable, 2D solitons may become stable in dipolar BECs for a sufficiently large dipole-dipole interaction (DDI) [4, 5]. Thus, the realization of dipolar BECs of chromium (Cr) [22, 23], dysprosium (Dy) [24] and erbium (Er) [25] opens fascinating perspectives for the realization of 2D BEC solitons. The realization of 2D solitons remains however an open challenge. On one hand the observation of the 2D solitons (for a dipolar orientation perpendicular to the soliton plane) proposed in Ref. [4] demands the inversion of the sign of the DDI by means of rotating fields [26]. On the other hand, anisotropic solitons, proposed in Ref. [5] for a dipolar orientation on the soliton plane, demand no external driving, but additional challenges may arise from their high anisotropy [27], in particular their vulnerability to collapse instability even in a strictly 2D scenario [28].

In this paper we study the effect of dipolar orientation with respect to the soliton plane (see Fig. 1) on the properties and stability of 2D bright solitons in dipolar BECs. Introducing the tilting angle α with respect to the normal vector of the quasi-2D trap plane [29–31] allows for accessing previously

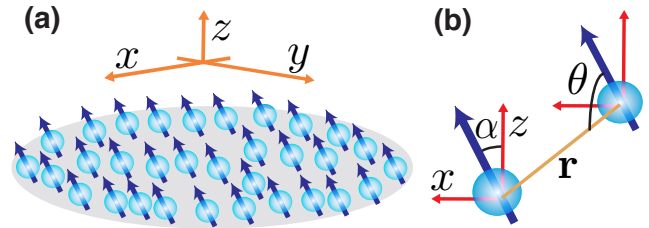


Figure 1. (a) The schematic setup of dipolar BEC confined in the xy plane with a strong harmonic confinement along the z axis. (b) The dipoles are polarized in the xz plane with tilting angle α w.r.t. z axis and θ is the angle between the dipole vector and the radial vector \mathbf{r} .

disregarded regimes of interaction parameters for soliton stability as well as to manipulate the soliton anisotropy in a more controlled manner. These features may enhance the possibilities of realizing 2D BEC solitons experimentally in the state-of-the-art dipolar BECs.

Solitons may be created by driving a BEC into phonon-instability (PI). This has been done in non-polar 1D BECs by tuning the short-range interactions from repulsive to attractive [21]. In contrast, in 2D and 3D PI leads to collapse in non-dipolar BECs [32, 33]. On the contrary, the post PI dynamics in 2D dipolar BECs is characterized by the formation of a transient gas of bright solitons [28]. The resulting solitons exhibit an intriguing dynamics that crucially depends on the nature of DDI on the soliton plane. Isotropic solitons attract each other in any direction, undergoing fusion during collisions and eventually becoming a single large soliton. The scenario is different for anisotropic solitons, as the interaction between the solitons is anisotropic in the plane, which makes them fuse only when they are colliding along the dipolar axis. Here we extend these studies to the tilted case. As we show, the post-PI dynamics is always characterized by a transient stripe pattern that eventually breaks into bright solitons.

The paper is structured as follows. In Sec. II we discuss the model and the corresponding non-local Gross-Pitaevskii

equations (NLGPEs). In Sec. III, we examine the Bogoliubov excitations of a 2D homogeneous BEC, identifying the regimes of PI as a function of the interaction parameters and the tilting angle. Sec. IV is devoted to analyzing the stability and the properties of the soliton. The stable/unstable regions of Cr, Er and Dy BECs are discussed as a function of system parameters. In Sec. V we demonstrate how to prepare a 2D soliton by varying the tilting angle from a soliton unstable to a soliton stable region in the case of a Cr BEC. Finally we conclude in Sec. VI.

II. MODEL

We consider a BEC of N particles with magnetic or electric dipole moment d , oriented in the xz plane forming an angle α with the z axis, using a sufficiently large external field (Fig. 1). The DDI potential is $V_d(\mathbf{r}) = g_d(1 - 3 \cos^2 \theta)/r^3$, where θ is the angle formed by the dipole vector $\mathbf{d} \equiv d(\sin \alpha \hat{x} + \cos \alpha \hat{z})$ and the radial vector \mathbf{r} , with $g_d \propto Nd^2$ being the strength of the dipole-potential. At low-enough temperatures the system is described by a non-local Gross-Pitaevskii equation (NLGPE):

$$i\hbar \frac{\partial}{\partial t} \Psi(\mathbf{r}, t) = \left[-\frac{\hbar^2}{2m} \nabla^2 + V_t(\mathbf{r}) + g|\Psi(\mathbf{r}, t)|^2 + \int d\mathbf{r}' V_d(\mathbf{r} - \mathbf{r}') |\Psi(\mathbf{r}', t)|^2 \right] \Psi(\mathbf{r}, t), \quad (1)$$

where $\int d\mathbf{r} |\Psi(\mathbf{r}, t)|^2 = 1$ and $g = 4\pi\hbar^2 aN/m$ is the coupling constant that characterizes the short-range contact interaction, with a the s -wave scattering length. Further, we assume a strong harmonic confinement along the z direction with a frequency ω_z and no trapping in the xy plane, hence $V_t(r) = m\omega_z z^2/2$. This trapping is sufficiently strong such that the system remains in the ground state, $\phi_0(z) = \exp(-z^2/l_z^2)/\sqrt{\pi^{1/2}l_z}$, of the harmonic oscillator along the z -axis with $l_z = \sqrt{\hbar/m\omega_z}$, factorizing the BEC wave function as $\Psi(\mathbf{r}) = \psi(x, y)\phi_0(z)$. In that case, the physics of dipolar BEC becomes quasi-2D, with the restriction that $|\mu_{2D}| \ll \hbar\omega_z$, where μ_{2D} is the chemical potential of the 2D gas. Employing this factorization, convolution theorem, the Fourier transform of the DDI potential,

$$\tilde{V}_d(\mathbf{k}) = \frac{4\pi g_d}{3} \left[\frac{3(k_x^2 \sin^2 \alpha + k_x k_z \sin 2\alpha + k_z^2 \cos^2 \alpha)}{k_\rho^2 + k_z^2} - 1 \right], \quad (2)$$

and integrating over dz , we get an effective 2D NLGPE:

$$i\hbar \frac{\partial}{\partial t} \psi(x, y, t) = \left[-\frac{\hbar^2}{2m} \nabla_{x,y}^2 + \frac{g}{\sqrt{2\pi}l_z} |\psi(x, y, t)|^2 + \frac{2g_d}{3l_z} \int \frac{dk_x dk_y}{(2\pi)^2} e^{i(k_x x + k_y y)} f(k_x, k_y) \tilde{n}(k_x, k_y) \right] \psi(x, y, t), \quad (3)$$

with $\tilde{n}(k_x, k_y)$ Fourier transform of $|\psi(x, y)|^2$ and

$$f(k, \theta_k) = \sqrt{2\pi} (3 \cos^2 \alpha - 1) + 3\pi e^{k^2/2} k \operatorname{erfc} \left(\frac{k}{\sqrt{2}} \right) \times (\sin^2 \alpha \cos^2 \theta_k - \cos^2 \alpha), \quad (4)$$

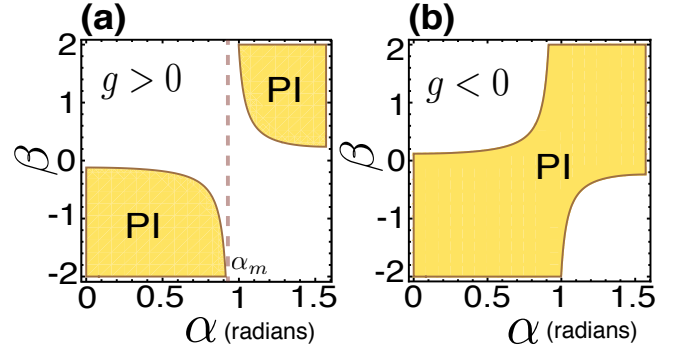


Figure 2. The PI regions (shaded) of a 2D dipolar BEC as a function of β and the tilting angle α (in radians) for (a) $g > 0$ and (b) $g < 0$. In the former case post PI dynamics is characterized by the formation of 2D solitons, while in the latter case the BEC becomes unstable against local collapses. The dashed line in Fig. 2(a) indicates the magic angle α_m across which the characteristics of DDI should be reversed in order to stabilize the 2D bright solitons.

where we use dimensionless polar coordinates ($k \equiv l_z \sqrt{k_x^2 + k_y^2}$ and θ_k), and $\operatorname{erfc}(x)$ is the complimentary error function. Note that for $\alpha = 0$ and $\alpha = \pi/2$ Eq. (3) reduces to the cases discussed in Refs. [4] and [28], respectively for the realization of isotropic and anisotropic solitons.

III. PHONON INSTABILITY

In this section, we calculate the low energy spectra (Bogoliubov excitations) of a 2D homogeneous dipolar BEC with tilted dipoles. The homogeneous solution of Eq. (3) is $\psi(x, y, t) = \sqrt{n_{2D}} \exp[-i\mu_{2D}t/\hbar]$, with n_{2D} the homogeneous 2D density. The 2D chemical potential is obtained as

$$\mu_{2D} = \frac{gn_{2D}}{\sqrt{2\pi}l_z} \left[1 + \frac{4\pi}{3} \beta (3 \cos^2 \alpha - 1) \right], \quad (5)$$

where $\beta = g_d/|g|$ determines the ratio between the DDI strength and that of the contact interactions. The elementary excitations of the homogeneous solution are of the form $\delta\psi_k(x, y, t) = u_k e^{-i(\mathbf{k}\cdot\mathbf{r} - \omega_k t)} + v_k^* e^{i(\mathbf{k}\cdot\mathbf{r} - \omega_k^* t)}$ with the dispersion

$$\epsilon_{\mathbf{k}} = \hbar\omega_{\mathbf{k}} = \sqrt{E_k \left\{ E_k + \frac{2gn_{2D}}{\sqrt{2\pi}l_z} \left[1 + \frac{2\sqrt{2\pi}}{3} \beta f(k) \right] \right\}}, \quad (6)$$

where $E_k = \hbar^2 (k_x^2 + k_y^2)/2m$. The phonon modes, $\epsilon(\mathbf{k} \rightarrow 0) \propto \sqrt{\mu_{2D}} k_\rho$ when $\mu_{2D} < 0$, which provides the PI condition:

$$g < -\frac{4\pi g_d}{3} (3 \cos^2 \alpha - 1). \quad (7)$$

For $g < 0$ PI always leads to local collapses, resembling the situation in BECs with short-range attractive interactions [32, 33] and in 3D homogeneous dipolar BECs [34, 35]. We hence focus below on BEC with repulsive contact interactions, $g > 0$, where PI arises due to the attractive part of the anisotropic

DDI. As shown in Ref. [28], for $\alpha = 0$ and $\alpha = \pi/2$ the post PI dynamics is characterized by the formation of a transient gas of bright solitons. The solitons then eventually undergo inelastic collisions, fusing together to form larger ones. The larger solitons may survive against collapse if the BEC density is low enough to hold the 2D criteria, $|\mu_{2D}| \ll \hbar\omega_z$.

The PI regions as a function of β and α with $g > 0$ (Fig. 2a) provide the first estimation for the stability regions of 2D bright solitons. In Fig. 2(a), there are two different regions in the α - β plane satisfying the PI criteria, separated at the *magic angle* $\alpha_m = 54.7$ degrees (or 0.95 radians). For $\alpha < \alpha_m$ the PI requires $g_d < 0$ which demands inverting the anisotropic character of DDI via rotating fields. This makes the direct cross-over between the two PI regions impossible by continuously varying α . Note that, in both regions, a sufficiently large $|\beta|$ may lead to local collapses. This introduces an upper cut-off for $|\beta|$ for the creation of stable solitons, which will be estimated in Sec. IV using variational calculations. Note from Fig. 2(a) that a dipolar BEC may be driven into PI just by tilting the dipoles from an initially stable configuration, without changing the interaction parameters or trap geometry. As it can be easily accomplished by changing the orientation of the externally applied field, we propose this as an alternative simple method to generate 2D bright solitons in dipolar BECs, combined with an adiabatic approach. This is numerically in-

vestigated in Sec. V.

IV. TWO DIMENSIONAL BRIGHT SOLITONS WITH TILTED DIPOLES

In this section, we analyze the stability of 2D solitons in a dipolar BEC with tilted dipoles, using a 3D variational solution and numerical NLGPE solutions.

A. Gaussian ansatz

We consider the following Gaussian ansatz:

$$\Psi_0(\mathbf{r}) = \frac{1}{\pi^{3/4} l_z^{3/2} \sqrt{L_x L_y L_z}} \exp\left[-\frac{1}{2l_z^2} \left(\frac{x^2}{L_x^2} + \frac{y^2}{L_y^2} + \frac{z^2}{L_z^2}\right)\right]. \quad (8)$$

The dimensionless variational parameters: L_x , L_y and L_z provide the Gaussian widths along x , y and z . Introducing this ansatz in the energy functional

$$E = \int d^3r \left[\frac{\hbar^2}{2m} |\nabla\Psi_0(r)|^2 + V_i(r)|\Psi_0(r)|^2 + \frac{g}{2} |\Psi_0(r)|^4 + \frac{1}{2} \int d^3r' V_d(r-r') |\Psi_0(r)|^2 |\Psi_0(r')|^2 \right],$$

we obtain

$$\begin{aligned} \frac{E}{\hbar\omega_z} = & \frac{1}{4L_x^2} + \frac{1}{4L_y^2} + \frac{1}{4L_z^2} + \frac{L_z^2}{4} + \frac{\tilde{g}}{4\pi L_x L_y L_z} + \frac{\tilde{g}_d}{3L_z} \left[\frac{3 \sin^2 \alpha}{L_x^2 - L_y^2} \left(\sqrt{\frac{L_y^2 - L_z^2}{L_x^2 - L_z^2}} - \frac{L_y}{L_x} \right) + \frac{3 \cos^2 \alpha}{\sqrt{(L_x^2 - L_z^2)(L_y^2 - L_z^2)}} - \frac{1}{L_x L_y} \right] \\ & - \frac{2\tilde{g}_d}{\pi} \int_0^{\pi/2} d\chi \frac{\cos^2 \chi \sin^2 \alpha - \cos^2 \alpha}{[L_z^2 - (L_x^2 \cos^2 \chi + L_y^2 \sin^2 \chi)]^{3/2}} \operatorname{arctanh} \left(\frac{\sqrt{L_z^2 - (L_x^2 \cos^2 \chi + L_y^2 \sin^2 \chi)}}{L_z} \right), \end{aligned} \quad (9)$$

where $\tilde{g} = g/\sqrt{2\pi\hbar\omega_z}l_z^3$ and $\tilde{g}_d = g_d/\sqrt{2\pi\hbar\omega_z}l_z^3$. The minimum of $E(L_x, L_y, L_z)$ provides the equilibrium widths $\{w_x^0, w_y^0, w_z^0\}$ of the soliton. The absence of this minimum results in two distinct types of instability. If the repulsive part of the interactions dominates, the soliton expands without limits on the xy plane ($w_{x,y}^0 \rightarrow \infty$), whereas dominating attractive interactions lead to collapse ($w_{x,y,z}^0 \rightarrow 0$).

B. Stability analysis and properties of 2D solitons

For $\alpha = 0$, we recover the isotropic scenario of Ref. [4], where stable isotropic solitons demand

$$\frac{2\tilde{g}_d}{3\sqrt{2\pi}} < 1 + \frac{\tilde{g}}{(2\pi)^{3/2}} < \frac{-4\tilde{g}_d}{3\sqrt{2\pi}}, \quad (10)$$

which requires $\tilde{g}_d < 0$, i.e. the inversion of the DDI. For large values of g , the above criteria reduces to $\beta < -3/8\pi$. Any $\alpha > 0$ breaks polar symmetry, and hence $w_x^0 \neq w_y^0$. We quantify the 2D soliton anisotropy with the aspect ratio $\gamma = w_i^0/w_j^0$, where $\{i, j\} \in \{x, y\}$ with $w_j^0 > w_i^0$ such that $\gamma \leq 1$.

For $\beta < 0$, increasing α from zero towards α_m leads to soliton elongation along y , $w_y^0 > w_x^0$, since the DDI becomes more attractive along y than along x , as schematically shown in Fig. 3a. In addition, both w_x^0 and w_y^0 increase monotonously with α since the overall attractive interaction is reduced. As shown in Fig. 3c, γ shows a non-monotonous character with a minimal value. Near the expansion instability, which happens at a \tilde{g} - and \tilde{g}_d -dependent angle $\alpha_e (< \alpha_m$ and shown by filled circles in Fig. 3c-f), the soliton anisotropy diminishes. The latter occurs because close to α_e both $w_{x,y}^0$ are very large, the interaction energy becomes hence very small, and as a result the

anisotropy diminishes. For $\beta > 0$, for $\alpha = \pi/2$ the solitons are maximally anisotropic with $w_x^0 > w_y^0$ for any value of \tilde{g} and \tilde{g}_d (see Fig. 3b). As expected, when α decreases from $\pi/2$, the anisotropy decreases monotonously, until instability against expansion occurs at a critical angle. Figures 3c (d) and 3e (f) show the results for different \tilde{g} (\tilde{g}_d) values with a fixed \tilde{g}_d (\tilde{g}). In both figures we show the results for γ obtained from the variation ansatz discussed above and from the numerical simulation of the 2D NLGPE, which are in excellent agreement in basically for all cases. As expected, the anisotropy increases with growing $|\tilde{g}_d/\tilde{g}|$. The fact that the values of \tilde{g} and \tilde{g}_d for with the 2D soliton is stable depend on the tilting angle α , allows for the observation of solitons in parameter regimes in which solitons are unstable either for $\alpha = 0$ [4] or $\alpha = \pi/2$ [5], hence easing the experimental realization of 2D solitons.

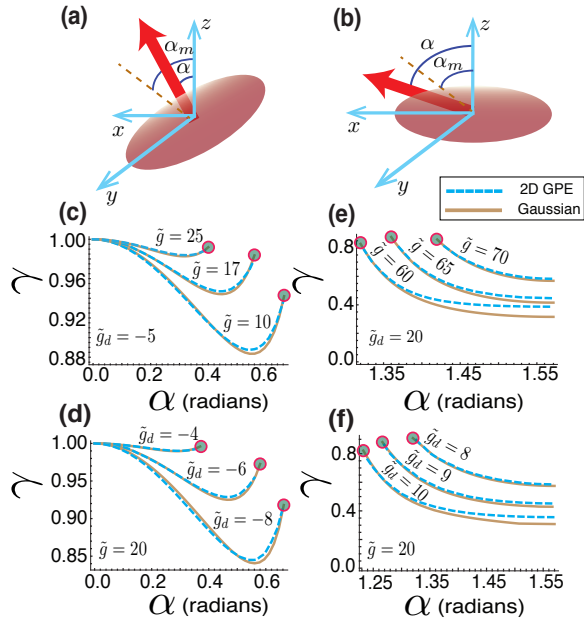


Figure 3. The figures (a) and (b) show the equilibrium configurations of the soliton for (i) $\beta < 0$ ($0 < \alpha < \alpha_m$) and (ii) $\beta > 0$ ($\alpha_m < \alpha \leq \pi/2$). The thick (red) arrow shows the orientation of the dipoles in the BEC. For the case (i) the soliton is more elongated along the y axis and hence the aspect ratio is taken as $\gamma = w_x^0/w_y^0$. In figures (c) and (d) γ as a function of α is shown for the case (i). The value of α at which each curves terminates ($\alpha = \alpha_e$), shown by filled circles, gives the critical angle for the expansion instability. For case (ii) the soliton is more elongated along the x axis, and hence we define $\gamma = w_y^0/w_x^0$, the corresponding plots as a function of α are shown in (e) and (f). In this case for $\alpha < \alpha_e$ the solitons are unstable against expansion.

C. Soliton gas formation after phonon instability

As mentioned above, PI in 2D dipolar BECs may be followed by the formation of a transient gas of bright solitons, instead of the collapse characteristic of short-range interacting BECs [28]. The post-instability evolution and the dynamics of the emergent soliton gas depend crucially on the tilting

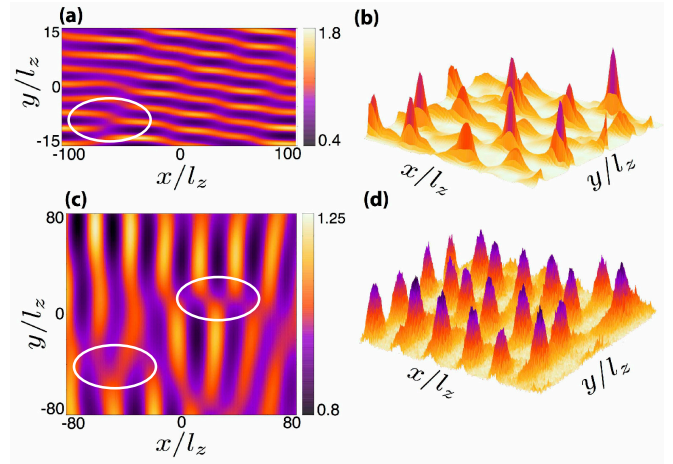


Figure 4. The snapshots of the post-PI dynamics in a 2D dipolar homogeneous condensate. The figures (a) and (b) are for $\tilde{g} = 12$, $\beta = 0.28$ and $\alpha = 1.35$ radians at times $t = 13.5/\omega_z$ and $t = 27/\omega_z$ respectively. Similarly, the figures (c) and (d) are for $\tilde{g} = 40$, $\beta = -0.29$ and $\alpha = 0.6$ radians at times $t = 31/\omega_z$ and $t = 90/\omega_z$ respectively. Figures (a) and (c) are the transient stripes patterns with the dislocation defects shown in ellipses. Figures (b) and (d) are the temporarily arranged, unstable, ordered state of the soliton gas, which eventually merge each other during collisions.

angle α . Figs. 4(a) and 4(b) show the post-instability density patterns for $\tilde{g} = 12$, $\beta = 0.28$ and $\alpha = 1.35$ radians at times $t = 13.5/\omega_z$ and $t = 27/\omega_z$, respectively. Note that the the first stages of the post-instability dynamics are characterized by the formation of a transient stripe pattern that present dislocation defects [36]. At these dislocations two stripes merge into one. Note that for the case considered the DDI is more attractive along the x -axis, which results in stripes almost parallel to the x direction. The initial formation of stripes is characteristic of in-plane anisotropy resulting from $\alpha > 0$. Stripes may be observed as well for $\beta < 0$, as illustrated in Figs. 4(c) and (d) for $\beta = -0.29$ and $\alpha = 0.6$ radians at timest $t = 31/\omega_z$ and $t = 90/\omega_z$, respectively. In this case, the DDI is more attractive along the y direction, resulting in stripes along the same direction. As shown in Fig. 4(b) and (d), the density stripes eventually break down into anisotropic solitons with major axis along the direction in which the DDI is more attractive, resulting in an unstable ordered state of solitons. The solitons eventually attract each other, fuse together and may remain stable depending on its condensate density. We have observed that the dynamics of the soliton gas inherently slowed down for $\alpha \neq 0$ compared to the isotropic case ($\alpha = 0$). This is because, in the latter case the attractive forces between the solitons are rotationally invariant, whereas in the former case it is dominant along one particular direction due to the anisotropy of DDI, which restricts the motion in other directions.

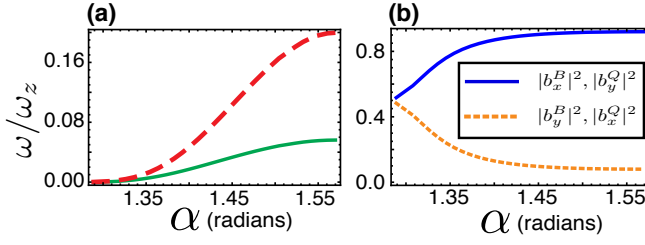


Figure 5. The eigen frequencies (a) and the square of the components of the eigen-vectors (b) of two low-lying xy modes for $\beta = 0.36$ as a function of α . For $\alpha = \pi/2$, the soliton is maximally anisotropic and the modes exhibit a pure x (solid lines) and y (dashed lines) character. As α reduces, the solitons become less anisotropic and near the expansion instability the modes turn into breathing and quadrupole like ones, akin to that of the isotropic case.

$$\mathcal{L} = \frac{i}{2}\hbar\left(\psi\frac{\partial\psi^*}{\partial t} - \psi^*\frac{\partial\psi}{\partial t}\right) + \frac{\hbar^2}{2m}|\nabla\psi(r,t)|^2 + V_i(r)|\psi(r,t)|^2 + \frac{g}{2}|\psi(r,t)|^2 + \frac{1}{2}|\psi(r,t)|^2 \int dr' V_d(r-r')|\psi(r',t)|^2.$$

The Lagrangian is then obtained by integrating over the whole space i.e., $L = \int d^3r \mathcal{L}$. We then obtain the corresponding Euler-Lagrange equations of motion for the time-dependent variational parameters, see App. A. Note that the centre of mass motion (along the z axis) is decoupled from the internal dynamics of the soliton. Below we analyze in detail the two in-plane (xy -) modes of the condensate, which lie lowest in the excitation spectrum. For $\alpha = 0$ (isotropic case), those are the breathing and quadrupole modes [4]. When $\alpha \neq 0$, the character of the in-plane modes change, and in particular as the anisotropy of the soliton increases the modes in the xy plane decouple into pure x and y modes. In order to visualize it, we plot the square of the components of the eigen-vectors $\mathbf{b} = b_x\hat{x} + b_y\hat{y}$ of the two planar modes for a particular case with $\beta = 0.36$, see Fig. 5(b) and the corresponding eigen-frequencies (ω) are shown in Fig. 5(a). For $\beta = 0.36$ and $\alpha = \pi/2$, the condensate is more elongated along the x -direction and hence the lowest mode (solid lines in Fig. 5) accounts mostly the oscillation of condensate width along the x -axis. When α reduces or dipoles tilting out of the xy plane, the anisotropy of the soliton decreases and the modes become more breathing-like (the lowest one) and quadrupole-like modes of the isotropic case, Fig. 5(b). Near the expansion instability they almost turn into breathing and quadrupole modes. The eigen-frequencies of the low lying modes are also crucial for the adiabatic control or preparation of the dipolar soliton, as discussed in Sec. V, where we have taken $\alpha \equiv \alpha(t)$. In particular, the frequency of the lowest mode determines the rate at which α should be varied in time in order for the system to remain in the instantaneous ground state of the system.

D. Variational Calculations : Low-lying excitations

At this point we examine the lowest-lying modes of 2D dipolar solitons using a variational method [37, 38], where we use a time-dependent Gaussian as the trial wave function:

$$\psi(x, y, z, t) = A(t) \prod_{\eta=x,y,z} e^{-\frac{(\eta-\eta_0(t))^2}{2w_\eta^2(t)}} e^{i\eta\alpha_\eta(t)} e^{i\eta^2\beta_\eta(t)}, \quad (11)$$

where η_0 , w_η , α_η and β_η are the time dependent variational parameters and the normalization constant $A(t) = \pi^{-3/4} / \sqrt{w_x w_y w_z}$. We consider the soliton is static in the xy plane and assume $x_0(t) = 0$ and $y_0(t) = 0$. The above ansatz is then introduced in the Lagrangian density of a dipolar BEC:

E. Experimentally Relevant atomic systems

Now we discuss the stability regions of the soliton in the state-of-the-art experimentally realized dipolar condensates of Cr, Dy and Er. In particular, we focus on the anisotropic solitons with $\beta > 0$, as it is experimentally less challenging. We take $\omega_z = 2\pi \times 1\text{kHz}$ and $N = 10000$, resulting in an effective dipolar interaction strengths of $\tilde{g}_d = 22$ (Cr), 170 (Er), 334 (Dy) for different atoms. The resulting phase diagrams obtained from Gaussian-energy calculations are shown in Fig. 6 as a function of the s -wave scattering length a and the tilting angle α . These phase diagrams are of considerable interest if one would like to tune the system from soliton unstable to soliton stable region either by tilting the dipoles orientation or tuning a using the Feshbach resonance. Below we demonstrate the adiabatic preparation of the soliton in a Cr BEC, using experimentally realistic parameters, by tuning the tilting angle in time in which the dipolar BEC undergoes the transition from externally confined BEC to a self trapped one.

V. ADIABATIC PREPARATION OF AN ANISOTROPIC BRIGHT SOLITON

The dependence of the BEC stability and of the soliton properties on the tilting angle α opens interesting perspectives for the preparation of 2D solitons by modifying in real time the tilting angle. In contrast to the previous sections we consider at this point the presence of an external shallow trap on the xy plane with frequencies $\omega_{x,y} = 2\pi \times 10\text{Hz}$. We consider a Cr-BEC of $N = 6000$ atoms with $\omega_z = 2\pi \times 1\text{kHz}$, initially prepared with a tilting angle $\alpha_i = 1.22$ radians and $a = 9a_0$, such that under these conditions there is no self-trapping (i.e. no 2D soliton), and the only confinement is provided by the xy trap. We may then keep the interaction parameters intact,

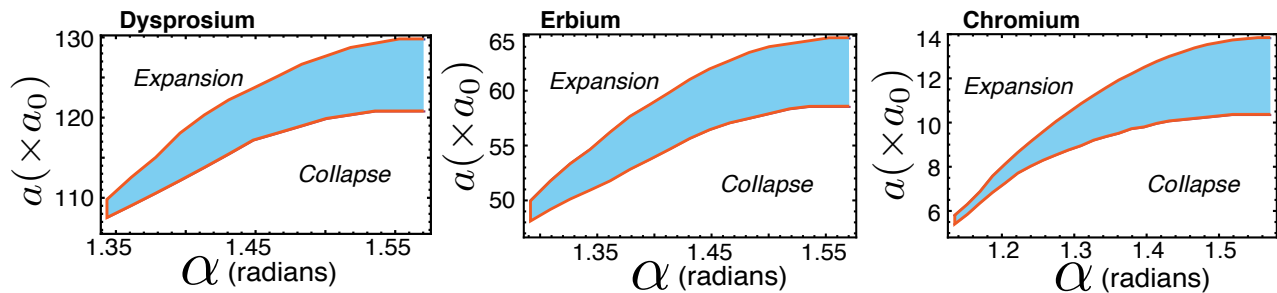


Figure 6. The stability regions (shaded) for the anisotropic solitons as a function of tilting angle α and the s -wave scattering length a (in units of Bohr radius a_0) for Dysprosium, Erbium and Chromium condensates, with $\omega_z = 2\pi \times 1\text{kHz}$ and $N = 10000$. The dipolar interaction is calculated with the intrinsic magnetic moments of each of the atoms. For large values of a the soliton become unstable against expansion and for lower values it undergoes the collapse instability.

and slowly tune α to a final value ($\alpha_f = 1.32$ radians) within the soliton-stability region. The trap on the xy plane may be then removed. The latter should be done slow-enough such that one avoids the significant creation of excitations in the condensate that may affect the self-trapping. The numerical results using the real-time evolution of the 2D NLGPE are shown in Fig. 7, where we monitor the widths of the condensate in the xy plane as function of time. The self-trapping of the condensate in the xy plane is evident from the periodic oscillation of the condensate widths, after the removal of the harmonic confinement. Note that the created soliton presents a slight breathing motion on the xy plane and the numerical results using the 2DGPE for the condensate density at various instants are shown in Fig. 7 a-c.

We can find different regimes of adiabaticity for the creation of bright soliton in dipolar BEC based on the different time scales in the system [39]. Here, we employ the condition $T_\omega \ll T \ll T_\mu$, where $T_\omega = \max\{1/\omega_B(\alpha(t))\}$, the equivalent of quantum mechanical linear adiabatic time scale, determined by the inverse of the lowest collective (breathing) mode ω_B and the nonlinear time scale $T_\mu = \max\{1/|\mu_{2D}(\alpha(t))|\}$ depends on the instantaneous chemical potential $\mu_{2D}(t)$. Note that in our case we vary the tilting angle from α_i to α_f in which the chemical potential changes from a positive to negative value continuously through $\mu_{2D} = 0$ ($T_\mu = \infty$). Thus the adiabatic criteria simply becomes $T_\omega \ll T$, which guarantee us that we do not significantly populate the excitations during the period T [40]. In the particular case considered here, $T_\omega \sim 0.05\text{s}$. The soliton preparation involves two steps, first in which we vary α and the second involves the removal of xy confinement, both done linearly in time. We varied α in 0.3s from α_i to α_f and the trap is then removed in a duration of 0.5s.

VI. CONCLUSIONS

In conclusion, we studied the physics of 2D bright solitons in dipolar condensates as a function of the orientation of the dipoles with respect to the soliton plane. As we showed, the tilting angle may enhance the experimental possibilities to observe the self-trapped matter waves as well as provide a probe

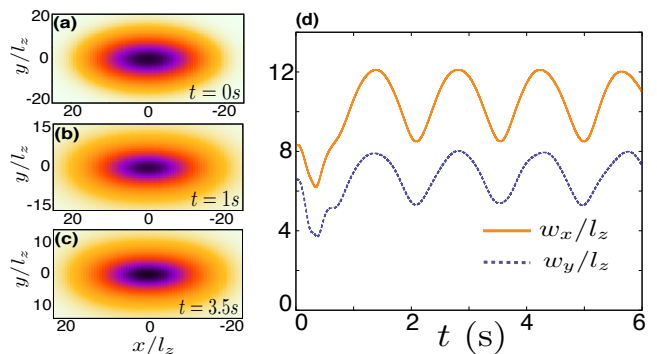


Figure 7. The numerical results of 2D GPE for the preparation of an anisotropic soliton starting from a weakly confined ($\omega_{x,y} = 2\pi \times 10\text{Hz}$) Cr BEC with $N = 6000$, $a = 9a_0$ and $\alpha = 1.22$ radians. (a) The initial condensate density, (b) after 1s and (c) after 3.5s. The tilting angle $\alpha(t)$ is varied linearly from $\alpha_i = 1.22$ to $\alpha_f = 1.32$ radians in 0.3s. Then, the trap in the xy plane is removed in 0.5s. (d) The widths w_x and w_y of the soliton along x and y directions respectively as a function of time. The periodic oscillation of the widths for $t > 0.8\text{s}$ indicates the self-trapping of the condensate.

to tune the anisotropy of the soliton. In addition, it can drive the dipolar BEC into PI without altering its interaction parameters or trap geometry. In 2D, the post PI dynamics is always characterized by a transient stripe formation and eventual formation of an unstable soliton gas. Finally we have demonstrated how to prepare the 2D soliton adiabatically by tuning the tilting angle in the case of a Cr BEC.

VII. ACKNOWLEDGMENTS

R. N and P. P acknowledge funding by the Indo-French Centre for the Promotion of Advanced Research - CEFIPRA. L.S. thanks the support of the Cluster QUEST, and the Deutsche Forschungsgemeinschaft (RTG 1729). M. R. acknowledges the funding from DST India through INSPIRE scholarship. Also, P. P. acknowledges financial support from Conseil Régional d'Ile-de-France under DIM Nano-K / IFRAF, CNRS, and from Ministère de l'Enseignement

Supérieur et de la Recherche within CPER Contract.

The above equations describe the motion of a particle with coordinates w_η in an effective potential

Appendix A: Lagrangian for a dipolar condensate

The Lagrangian density for a dipolar condensate is given in Eq. 12, and using the Gaussian time-dependent trial function we obtain the Lagrangian $L = \int d^3r \mathcal{L}$:

$$L = \sum_{\eta=x,y,z} \left[\hbar \frac{\dot{\beta}_\eta w_\eta^2}{2} + \frac{\hbar^2}{2m} \left(\frac{1}{2w_\eta^2} + \alpha_\eta^2 + 2\beta_\eta^2 w_\eta^2 \right) \right] + \frac{1}{2} m \omega_z^2 \frac{w_z^2}{2} + \frac{g}{\sqrt{2\pi}} \frac{1}{4\pi w_x w_y w_z} + V(w_\eta), \quad (\text{A1})$$

where

$$V(w_\eta) = \frac{1}{2} \frac{1}{(2\pi)^3} \int d^3k \tilde{V}_d(\mathbf{k}) \prod_{\eta=x,y,z} e^{-\frac{k_\eta^2 w_\eta^2}{2}} \quad (\text{A2})$$

with $\tilde{V}_d(\mathbf{k})$ the Fourier transform the dipole-dipole potential. Then, the equations of motion for the condensate widths are obtained as

$$m\dot{w}_x = \frac{\hbar^2}{mw_x^3} + \frac{g}{(2\pi)^{3/2} w_x^2 w_y w_z} - 2 \frac{\partial V}{\partial w_x} \quad (\text{A3})$$

$$m\dot{w}_y = \frac{\hbar^2}{mw_y^3} + \frac{g}{(2\pi)^{3/2} w_x w_y^2 w_z} - 2 \frac{\partial V}{\partial w_y} \quad (\text{A4})$$

$$m\dot{w}_z = \frac{\hbar^2}{mw_z^3} + \frac{g}{(2\pi)^{3/2} w_x w_y w_z^2} - m\omega_z^2 z^2 - 2 \frac{\partial V}{\partial w_z}. \quad (\text{A5})$$

$$U(W_\eta) = \frac{\hbar^2}{2m} \sum_{\eta} \frac{1}{w_\eta^2} + \frac{1}{2} m \omega_z^2 w_z^2 + \frac{g}{(2\pi)^{3/2} w_x w_y w_z} + V(w_\eta). \quad (\text{A6})$$

Once the equilibrium widths of the condensate are obtained by minimizing the effective potential (or equivalently from the Gaussian energy calculations in Section. IV A), the low lying excitations are obtained by diagonalizing the Hessian matrix of U . Also, note that the centre of mass motion of the soliton along the z axis is de-coupled from the internal dynamics and is governed by the equation

$$\ddot{z}_0 = -\omega_z^2 z_0. \quad (\text{A7})$$

-
- [1] A. W. Snyder and D. J. Mitchell, *Science* **276**, 1538 (1997).
[2] O. Bang, W. Krolikowski, J. Wyller, and J. J. Rasmussen, *Phys. Rev. E* **66**, 046619 (2002).
[3] A. Alberucci, C. P. Jisha, N. F. Smyth, and G. Assanto, *Phys. Rev. A* **91**, 013841 (2015).
[4] P. Pedri and L. Santos, *Phys. Rev. Lett.* **95**, 200404 (2005).
[5] I. Tikhonenkov, B. A. Malomed, and A. Vardi, *Phys. Rev. Lett.* **100**, 090406 (2008).
[6] F. Maucher, N. Henkel, M. Saffman, W. Królikowski, S. Skupin, and T. Pohl, *Phys. Rev. Lett.* **106**, 170401 (2011).
[7] M.-f. Shih, M. Segev, and G. Salamo, *Phys. Rev. Lett.* **78**, 2551 (1997).
[8] C. Conti, M. Peccianti, and G. Assanto, *Phys. Rev. Lett.* **91**, 073901 (2003).
[9] M. Peccianti and G. Assanto, *Physics Reports* **516**, 147 (2012).
[10] Y. Lamhot, A. Barak, O. Peleg, and M. Segev, *Phys. Rev. Lett.* **105**, 163906 (2010).
[11] A. Butsch, C. Conti, F. Biancalana, and P. S. J. Russell, *Phys. Rev. Lett.* **108**, 093903 (2012).
[12] W. Man, S. Fardad, Z. Zhang, J. Prakash, M. Lau, P. Zhang, M. Heinrich, D. N. Christodoulides, and Z. Chen, *Phys. Rev. Lett.* **111**, 218302 (2013).
[13] C. Conti, M. Peccianti, and G. Assanto, *Phys. Rev. Lett.* **92**, 113902 (2004).
[14] S. Minardi, F. Eilenberger, Y. V. Kartashov, A. Szameit, U. Röpke, J. Kobelke, K. Schuster, H. Bartelt, S. Nolte, L. Torner, et al., *Phys. Rev. Lett.* **105**, 263901 (2010).
[15] R. Nath, P. Pedri, and L. Santos, *Phys. Rev. A* **76**, 013606 (2007).
[16] R. Eichler, D. Zajec, P. Köberle, J. Main, and G. Wunner, *Phys. Rev. A* **86**, 053611 (2012).
[17] K. Łakomy, R. Nath, and L. Santos, *Phys. Rev. A* **85**, 033618 (2012).
[18] S. Skupin, M. Saffman, and W. Królikowski, *Phys. Rev. Lett.* **98**, 263902 (2007).
[19] L. Khaykovich, F. Schreck, G. Ferrari, T. Bourdel, J. Cubizolles, L. D. Carr, Y. Castin, and C. Salomon, *Science* **296**, 1290 (2002).
[20] K. E. Strecker, G. B. Partridge, A. G. Truscott, and R. G. Hulet, *Nature* **417**, 150 (2002).
[21] S. L. Cornish, S. T. Thompson, and C. E. Wieman, *Phys. Rev. Lett.* **96**, 170401 (2006).
[22] A. Griesmaier, J. Werner, S. Hensler, J. Stuhler, and T. Pfau, *Phys. Rev. Lett.* **94**, 160401 (2005).
[23] Q. Beaufils, R. Chircireanu, T. Zanon, B. Laburthe-Tolra, E. Maréchal, L. Vernac, J.-C. Keller, and O. Gorceix, *Phys. Rev. A* **77**, 061601 (2008).
[24] M. Lu, N. Q. Burdick, S. H. Youn, and B. L. Lev, *Phys. Rev. Lett.* **107**, 190401 (2011).

- [25] K. Aikawa, A. Frisch, M. Mark, S. Baier, A. Rietzler, R. Grimm, and F. Ferlaino, *Phys. Rev. Lett.* **108**, 210401 (2012).
- [26] S. Giovanazzi, A. Görlitz, and T. Pfau, *Phys. Rev. Lett.* **89**, 130401 (2002).
- [27] P. Köberle, D. Zajec, G. Wunner, and B. A. Malomed, *Phys. Rev. A* **85**, 023630 (2012).
- [28] R. Nath, P. Pedri, and L. Santos, *Phys. Rev. Lett.* **102**, 050401 (2009).
- [29] A. K. Fedorov, I. L. Kurbakov, Y. E. Shchadilova, and Y. E. Lozovik, *Phys. Rev. A* **90**, 043616 (2014).
- [30] A. Macia, J. Boronat, and F. Mazzanti, *Phys. Rev. A* **90**, 061601 (2014).
- [31] D. Baillie and P. B. Blakie, *New Journal of Physics* **17**, 033028 (2015).
- [32] E. A. Donley, N. R. Claussen, S. L. Cornish, J. L. Roberts, E. A. Cornell, and C. E. Wieman, *Nature* **412**, 295 (2001).
- [33] J. M. Gerton, D. Strekalov, I. Prodan, and R. G. Hulet, *Nature* **408**, 692 (2000).
- [34] T. Lahaye, C. Menotti, L. Santos, M. Lewenstein, and T. Pfau, *Reports on Progress in Physics* **72**, 126401 (2009).
- [35] L. Santos, G. V. Shlyapnikov, P. Zoller, and M. Lewenstein, *Phys. Rev. Lett.* **85**, 1791 (2000).
- [36] R. Hoyle, *Pattern Formation* (Cambridge university press, 2006).
- [37] V. M. Pérez-García, H. Michinel, J. I. Cirac, M. Lewenstein, and P. Zoller, *Phys. Rev. Lett.* **77**, 5320 (1996).
- [38] S. Yi and L. You, *Phys. Rev. A* **63**, 053607 (2001).
- [39] Y. B. Band, B. Malomed, and M. Trippenbach, *Phys. Rev. A* **65**, 033607 (2002).
- [40] H. Pu, P. Maenner, W. Zhang, and H. Y. Ling, *Phys. Rev. Lett.* **98**, 050406 (2007).